Journal of the Brazilian Society of Mechanical Sciences and Engineering (2021) 43:30
https://doi.org/10.1007/s40430-020-02757-w

TECHNICAL PAPER

A numerical solution of the wave–body interactions for a freely floating vertical cylinder in different water depths using OpenFOAM

Mahdi Yousefifard[1] · **Adeleh Graylee**[1]

Received: 15 November 2019 / Accepted: 30 November 2020 / Published online: 3 January 2021

Abstract
In the present study, a finite volume method based on Reynolds-averaged Navier–Stokes equations is developed numerically in OpenFOAM to simulate two-phase flows around a freely floating cylinder in a numerical wave tank (NWT). All numerical computations are carried out using interDyMFoam solver, manipulating dynamic mesh. The left wall of NWT oscillates as a paddle wave-maker to produce desired waves. The accuracy of the current numerical method is confirmed by evaluating the results of some published experimental benchmarks, including the generation of regular waves in NWT and also the response of two fixed and floating objects in waves. Based on the current study findings, OpenFOAM is capable of predicting these cases of wave–structure interaction with good delicacy. Additionally, the moving wall of NWT as a flap-type wave-maker can produce waves with different attributes sufficiently. In the following, the influence of regular waves on a circular cylinder, operating freely in deep water, as well as the effect of the water depth on the cylinder's movement and forces acting on it are assessed. The results indicated that the change in the water depth has a significant effect on the response of the freely floating cylinder in waves.

Keywords CFD · RANS equations · OpenFOAM · Floating cylinder · Regular waves · Shallow water

1 Introduction

Nowadays, adopting fixed and floating structures with simple geometries has widely increased in the analysis of offshore problems. Designing new complex floating structures requires detailed knowledge about displacements and rotations of floating objects, flow directions, velocities around them, and also forces acting on these kinds of structures. In recent years, there has been a great deal of research into wave generation in a NWT and accurate evaluation of fluid flow and floating object dynamics. The reason for such simulations is that more sophisticated techniques can be used with more powerful computers. Lower-order solutions, capturing the effect of interaction between waves and floating objects, can be obtained with an analytical formulation based on potential theory, assuming that the fluid is inviscid, the flow is irrotational, and the wave has a small amplitude. Ghadimi et al. [1] found an analytical solution for the boundary volume problem of a floating vertical circular cylinder to evaluate the wave loads on the cylinder with heave and pitch motions in the water of finite depth in the presence of incident waves. In other studies, Finnegan et al. [2, 3] carried out that the potential velocity was solved by the method of separation of variables to construct approximate analytical expressions for wave excitation forces, considering the wave scattering problem, acting on a fixed and floating truncated vertical cylinder in the water of infinite depth. Yao et al. [4] investigated the influence of a bottom-mounted obstacle on forces acting on a fixed circular cylinder using the methods of variables separation and eigenfunction expansion for velocity potentials. The limitation of analytical formulae is that they have to be modified to deal with different scenarios. Besides, increasing the complexity in the design of structures and the need for a more accurate estimation of the hydrodynamic coefficients, numerical techniques such as boundary element method (BEM) and finite volume method (FVM) have been applied in hydrodynamic assessments. In fact, numerical methods become interesting, not only from a

Technical Editor: Celso Kazuyuki Morooka.

✉ Mahdi Yousefifard
yousefifard@nit.ac.ir

[1] Department of Mechanical Engineering, Babol Noshirvani University of Technology, Shariati Ave., Babol 47148-71167, Iran

financial matter but also from a performance point of view, as an extra input or a full alternative to the experiments. In one report [5], nonlinear interactions between large waves and a freely floating box with a spring-type mooring were investigated using a 2D fully nonlinear numerical wave tank based on potential theory, MEL/material-node time-marching approach, and BEM. The higher-order boundary element method, as a common approach of the solution, was used in some investigations [6–8] to solve the mixed boundary value problem at each time step to simulate wave–body interaction issues. Song et al. [9] employed the moving particle semi-implicit method (MPS) to find the solution of mass and momentum conservation equations for an incompressible fluid around a fixed cylinder located in the intermediate and deep water. However, few studies have considered a fluid flow with real properties such as viscosity and free surface effect. Nowadays, these phenomena have been increasingly investigated using CFD methods. Zhao and Hu [10] provided an experimental and numerical study on a simple box-shaped geometry with a rectangular superstructure dealing with regular and focused waves and a combination of them. Their computations were performed employing a constrained interpolation profile (CIP)-based Cartesian grid method based on Navier–Stokes equations to analyze the nonlinear wave–structure interaction. In another investigation [11], the wave run-up around a fixed circular and square cylinder exposing small-amplitude waves was obtained experimentally and numerically using FLUENT software. Also, Nematbakhsh et al. [12] assessed some benchmarks, including a fixed surface-piercing cylinder and a box that was limited in sway direction using the CFD-based numerical wave tank, to work on the reaction of bodies in small-amplitude waves.

Using the time-averaged forms of the non-dimensionalized continuity and momentum equations creates the basis of RANS model. In order to conduct the numerical simulation, Lin et al. [13] developed a CFD model based on the commercial software FLUENT, using a RANS solver for incompressible fluid flows and employed k-ε turbulent closure, to survey the wave run-up around three types of wind turbine foundations which were fixed at the bottom of the fluid domain. A benchmark, including the comprehensive investigation of the behavior of a submerged spherical wave energy converter (WEC) in waves and also responses of waves via the movement of WEC, was carried out experimentally and numerically by Bharath et al. [14]. The numerical simulations were conducted using the commercial CFD tool FLUENT based on RANS equations. In recent years, using OpenFOAM as an innovative numerical tool has attracted the attention of many researchers. Open-source Field Operation And Manipulation (OpenFOAM) has been considered as a powerful code to analyze problems in the field of wave–body interaction. Chen et al. [15] investigated the interaction of nonlinear regular and focused waves with a vertical cylinder in OpenFOAM. They used the InterFOAM solver to study wave responses around the fixed vertical cylinder up to at least fourth-order harmonic. Chen and Zhou [16] studied the horizontal force acting on a bottom-mounted vertical cylinder in deep and intermediate water depth using OpenFOAM solver, InterFOAM. The interaction of regular waves with a fixed and floating vertical cylinder, moving only vertically, was carried out in OpenFOAM by Hu et al. [17]. They used InterFOAM and interDyMFoam solvers and also the waves2Foam library, as an inlet boundary condition, to represent the extreme wave event together with first- or second-order Stokes wave theories for individual wave components. The mentioned new boundary condition was implemented on a fixed and floating cylinder and an FPSO in extreme waves. Ye and Wan [18] studied a turbulence flow field around a fixed cylinder using the PimpleFoam solver provided by OpenFOAM to assess the vortex-induced vibration. Nowadays, the ability of OpenFOAM in the simulation of the real condition of fluids and solution environments is of interest to many researchers for the dynamic analysis of ship and offshore structures [19, 20].

According to the investigations mentioned above, in general, floating offshore structures are completely fixed or partially floating in the sea. As a result, the influence of the structure motion on the wave run-up has seldom been reported. Not many examinations have been fulfilled on objects maneuvering in water with no movement restriction, especially considering real characteristics of flow such as viscosity, surface tension, free surface effect, etc. However, the results obtained from laboratory procedures, analyzing fixed and semi-moving structures in waves, can be used as a benchmark to confirm the results of numerical methods [10, 21, 22]. On the other hand, progress in computing power has led to the use of more complicated methods to solve such problems. In fact, a lot of research is still being done to evaluate the accuracy of the wave produced in a NWT [23].

The works mentioned above that used OpenFOAM software have been about fixed structures in a current. InterDyMFoam solver provides a simple tool for generating waves in a current. Therefore, using this solver to analyze the dynamic movement of a floating object in a place far from the wave-maker is not easily possible. What distinguishes this study from similar researches is the method of wave generation as well as the accuracy of the wave propagating along the NWT. Also, the use of the moving mesh technique in wave-maker and moving object simultaneously is one of the remarkable points of this research. The difference between the dynamic mesh technique used in this study and other methods such as slider mesh is that in the present method, the total number of cells in the solution domain is

constant during the numerical solution process. Of course, such an approach offers more acceptable performance for problems involving limited displacements [24, 25].

The purpose of the present paper is to evaluate the capability of the new form of paddle wave-maker to generate waves with the desired characteristic. To confirm this issue, the result of some published experimental benchmarks, including wave generation in NWT and the analysis of some fixed and floating objects in waves, is compared with the result of the current numerical method. The most important challenge is the simultaneous analysis of the free surface fluctuation of water and the displacement of the floating object. Therefore, one of the requirements of this research is the production of a precise NWT with generating desired waves. Also, the dynamic mesh technique should be used to accurately evaluate the dynamic movements of the object. It has been carried out based on RANS equations solved by FVM.

To demonstrate the methodology, a vertical truncated circular cylinder will be studied in deep water. At the first step, the ability of a flap-type wave-maker, generating proper waves using the movement of the left boundary, is investigated and validated with experimental data [10]. In the next step, a fixed cylinder based on the Ocean Engineering Committee [21] and a freely floating box according to the setup of Ming et al. [22] are analyzed in regular waves, and the surge and heave motions of those bodies are compared with experimental ones to verify the accuracy of the present numerical method. Finally, a freely floating circular cylinder is assessed in regular waves. The process of variation of surge and heave motions and horizontal and vertical forces acting on the cylinder via the change in the depth of water are estimated and presented.

2 Numerical model

The computational domain for FSI problems consists of the fluid and structure. In this work, the velocity u and pressure p are considered, as the unknown variables of the fluid flow field. For the structural part, the displacement and force are chosen, as the unknown field variable for a rigid body.

2.1 Governing equation

RANS equations can be used based on the knowledge of properties of the flow turbulence to give approximate time-averaged solutions to Navier–Stokes equations. Incompressible RANS equations are discretized in the fluid domain using FVM while capturing the free surface effect via the VOF method. In terms of an incompressible fluid, RANS equations are written as mass conservation equations and momentum conservation equations using Cartesian tensor notation. The continuity equation and the tensorial form of the RANS equation, which link pressure and velocity, can be written as [24]:

Continuity:

$$\frac{\partial U_i}{\partial x_i} = 0. \tag{1}$$

Momentum:

$$\frac{\partial U_i}{\partial t} + U_j \frac{\partial U_i}{\partial x_j} = \frac{\partial}{\partial x_j}\left(\nu \frac{\partial U_i}{\partial x_j} - \overline{u_i u_j}\right) - \frac{1}{\rho}\frac{\partial p}{\partial x_i}, \tag{2}$$

where U_i is the mean-velocity vector, u_i is fluctuating velocity, p is the pressure, υ and ρ are kinematic viscosity and density, respectively. The turbulence correlations, $u_i u_j$ that appear in Eq. (2), are unknown Reynolds stresses approximated by the turbulence closure. The turbulence closure used in this study is of the eddy-viscosity-type and is based on Boussinesq's assumption of linear stress–strain relationship to determine unknown Reynolds stresses.

$$\overline{u_i u_j} = \nu_t \left(\frac{\partial U_i}{\partial x_j} + \frac{\partial U_j}{\partial x_i}\right) - \frac{2}{3}\delta_{ij} k, \tag{3}$$

where υ_t is the eddy viscosity, in this study, determined by reference to the turbulent kinetic energy (k) and its rate of dissipation by viscous action (ε).

$$\nu_t = C_\mu \frac{k^2}{\varepsilon}, \tag{4}$$

Where C_μ is a coefficient determined by reference to the experimental data, k and ε are obtained from the solution of their own transport equations which are given by:

$$\frac{\partial k}{\partial t} + U_j \frac{\partial k}{\partial x_j} = \frac{\partial}{\partial x_j}\left[\left(\nu + \frac{\nu_t}{\sigma_k}\right)\frac{\partial k}{\partial x_j}\right] + P_k - \varepsilon, \tag{5}$$

$$\frac{\partial \varepsilon}{\partial t} + U_j \frac{\partial \varepsilon}{\partial x_j} = \frac{\partial}{\partial x_j}\left[\left(\nu + \frac{\nu_t}{\sigma_\varepsilon}\right)\frac{\partial \varepsilon}{\partial x_j}\right] + C_{\varepsilon 1}\frac{\varepsilon}{k}P_{\mathrm{k}} - C_{\varepsilon 2}\frac{\varepsilon^2}{k}, \tag{6}$$

where P_{k} is the rate of production of the turbulent kinetic energy.

$$P_k = \nu_t \frac{\partial U_i}{\partial x_j}\left(\frac{\partial U_i}{\partial x_j} + \frac{\partial U_j}{\partial x_i}\right) \tag{7}$$

The value of all the coefficients is presented in Table 1. An additional equation must also be taken into account to describe the movement of phases. Since, in the vast majority of coastal engineering applications, only water and air are presented, the following analysis is carried out for those two phases.

Table 1 Model coefficients

Model type	C_μ	σ_k	σ_ε	$C_{\varepsilon 1}$	$C_{\varepsilon 2}$	ρ_a(kg/m$^{3)}$	ρ_w (kg/m$^{3)}$
$k-\varepsilon$	0.09	1	1.3	1.44	1.92	1	1025

The numerical analysis has been carried out using interDyMFoam, a two-phase flow solver built on the OpenFOAM platform, tracking the free surface evolution utilizing a VOF technique. Here, a scalar indicator function between zero and one, known as volume fraction, is used to distinguish between two different fluids. The free surface is treated as the transitional layer between the two fluids. The volume (phase) fraction equation is presented below in which α represents the volume (phase) fraction, t represents time, and U refers to velocity. If $\alpha=1$, the cell is full of water, if $\alpha=0$, the cell is full of air, and in any other case it belongs to the interface [26]:

$$\frac{\partial \alpha}{\partial \mathrm{t}} + \nabla \cdot (\alpha U) = 0 \tag{8}$$

The interface between the two fluids requires special treatment to maintain a sharp interface; numerical diffusion would otherwise mix the two fluids over the whole domain. The tracking of the interface between the phases is accomplished by solving the continuity equation for the volume fraction of the second phase. Here, a mass does not move at the boundary of two fluids, and for this reason, the right-hand side of this equation is zero.

The volume fraction α is used to determine the density, viscosity and velocity of the mixture inside each cell of the mesh as shown in Eq. (9) [27].

$$\rho = \alpha \rho_{\mathrm{w}} + (1-\alpha)\rho_{\mathrm{a}}, \tag{9-a}$$

$$\mu = \alpha \mu_w + (1-\alpha)\mu_a, \tag{9-b}$$

while w and a represent water and air, respectively.

The equation for the motion of the body is given as [28]:

$$\sum_{i=0}^{3} F_i = ma_i, \tag{10}$$

where m represents the mass of the body, F is the resultant force acting on the body, and a_i is the velocity vector of the center of mass. An angular momentum equation of the body is formulated in the body local coordinate system with the origin in the center of the body:

$$\sum_{i=1}^{3} M_i = I\vartheta_i, \tag{11}$$

here, I denotes the inertia, ϑ is the angular acceleration of the rigid body, M is the resultant moment acting on the body, and i shows the DOF. By integrating the translational and angular acceleration over the time step, we get the current linear and angular velocities:

$$v_{i\mathrm{new}} = \int_{t_{\mathrm{old}}}^{t_{\mathrm{new}}} a\mathrm{d}t = v_{i\mathrm{old}} + a_i \Delta t, \tag{12}$$

$$w_{i\mathrm{new}} = \int_{t_{\mathrm{old}}}^{t_{\mathrm{new}}} \vartheta \mathrm{d}t = \omega_{i\mathrm{old}} + \vartheta_i \Delta t. \tag{13}$$

From the new velocities, the angle rotated and the distance traveled can get from the last time step. In the current study, both fixed objects and bodies with 6-DOF have been evaluated. It includes translate and rotate along all three axes in a 3-D system. The movements of the body have been estimated according to the computed velocity and pressure fields in the flow domain.

2.2 Solution procedure

The discretization method used in the CFD model to solve RANS equations is based on the finite volume method (FVM), which is an approach for representing and evaluating partial differential equations (PDEs) in the form of algebraic equations. VOF method has been applied in OpenFOAM to track free surface in problems involving two fluids with a common interface. FVM is a numerical technique transforming partial differential equations, representing conservation laws over differential volumes, into discrete algebraic equations over finite cells. In a similar fashion to finite difference (FDM) or finite element method (FEM), the first step in the solution process is the discretization of the domain, which in the FVM is discretized into non-overlapping elements or finite volumes.

Software Rhino 5 has been utilized to create a plan of floating objects. Simulated structures were transferred to OpenFOAM as a stl-format file. OpenFOAM is capable of analyzing the interaction between floating objects and the seawater. The customizable nature of the OpenFOAM software and the accuracy of the result have made it a popular choice for users wishing to have a degree of control over the physics and computational parts of the problem [26]. The solver employed in this study is interDyMFoam. It solves the 3D Reynolds-averaged Navier–Stokes (RANS) equations for two incompressible phases, using a finite volume discretization and the volume of fluid (VOF) method, and it handles dynamic meshes.

The interDyMFoam solver is an extended version of the InterFoam solver that can analyze problems involving limited mesh movement using a dynamic mesh technique based on a fixed number of cells. The interDyMFoam is capable of producing automatic mesh motion, as well as topological changes to the mesh such as addition or removal of a cell layer, boundaries that can be attached and detached, and a sliding interface, where a pair of detached surfaces move relative to each other.

There are two methods for numerically simulating moving objects using the dynamic mesh technique: moving mesh and sliding mesh. Using the sliding mesh method requires more time and cost and is therefore used for problems that involve large displacements; like simulating ship maneuvering. However, in this research, a moving mesh has been used, and due to the limited displacements in relation to the dimensions of the solution domain, acceptable results have also been obtained. In this method, the number of cells is constant and the deformation of each cell is applied automatically. Mesh refinement around the moving object as well as the free surface region is performed by the software's default function.

Moving mesh in OpenFOAM is managed through the dynamicMotionSolverFvMesh function. This solver morphs the mesh around a specified set of boundaries. The meshing motion is calculated based on the pressures on those boundaries. In turn, the dynamicMotionSolverFvMesh provides feedback to the fluid simulation. This mesh control is almost exclusively used to solve problems involving rigid body motion. A 6-DOF solid body can be specified through a boundary condition on a patch, prescribing the boundary of the solid body. With the moving mesh method, the mesh quality around the body is preserved, without performing expensive re-meshing, even when simulating arbitrary angles of rotation. As it is not possible to move only a few points in the mesh without destroying the shape of the cells, the neighboring points need to be moved as well, and this is done by the motionFvSolvers by a diffusion algorithm.

To simulate a problem numerically in OpenFOAM, it is needed to model a numerical wave tank (NWT). For this purpose, in the current examination, a 3D rectangular prism with a length of L, the width of W, and height of H is selected as a wave tank and bounded with an inlet (wave-maker), outlet, bottom, atmosphere, and front and back boundaries. All simulations were initialized to begin each simulation with water below the still water level and the air above the still water level. A sleepy sloped structure is added to the end of the wave tank, with a proper distance from the outlet, to absorb the energy of the waves and prevent wave reflection. The left boundary oscillates like a paddle from the bottom of the tank with constant amplitude and speed to generate intended waves (Fig. 1 and Table 2). The coordinate system has modeled considering the Cartesian coordinate with the positive z-axis in the vertical direction and the origin (0, 0, 0) located on the free surface. The uniform value of zero only applies to the initialization of all cases. The maximum Courant number is set to be 0.5. The initial time step is set to be 0.01 s and is modified automatically according to the Courant number.

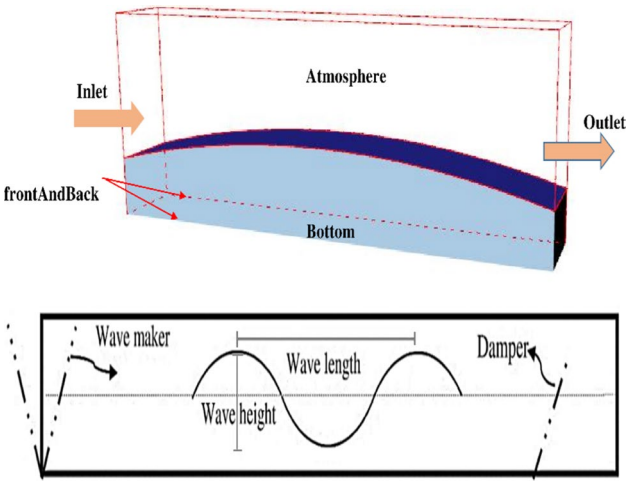

Fig. 1 Schematic of computational domain in NWT

In Table 2, Alpha1 is the volume fraction of phase 1 (water), P_rgh is the total pressure considering the hydrostatic pressure, and U is the fluid field velocity.

3 Validation

In order to certify the capability of the current procedure, three different examples, including one case for the wave-maker approval and two cases for the interaction of regular waves and a fixed circular cylinder and a freely floating box, are investigated, and the results have been compared with experimental data. It should be noted that the simulation of the cylinder in the numerical wave tank with a scale of 1:50.3 has been done.

3.1 Wave generation

Wave generation always plays a critical role in the vast majority of cases researchers are challenging. In this study, the wave is produced in a 3D NWT with the length of 16 m, the width of 0.3 m, and a height of 1 m. The inlet boundary of the numerical wave tank oscillates with a constant amplitude and angular velocity and creates accurate harmonious waves. To prevent the reflection of the wave from the end wall of the tank, two methods have been used simultaneously. A real damper with a 60° slope and a hollow surface is placed at the end of the tank to simulate a laboratory-like environment. In addition, a coarser mesh is used in the areas close to the damper, which

Table 2 Boundary conditions of NWT

Boundary	Alpha1	P_rgh	U
Inlet	zeroGradient	buoyantPressure	movingWallVelocity
Outlet	zeroGradient	buoyantPressure	fixedValue
Bottom	zeroGradient	buoyantPressure	fixedValue
Atmosphere	inletOutlet	totalPressure	pressureInletOutletVelocity
frontAndBack	zeroGradient	buoyantPressure	fixedValue

causes the wave propagating in that area to be dissipated. The transfer function of the current wave-maker is introduced in Eq (12).

$$Tr = \frac{\text{wave height}}{\text{wave maker stroke}} = \frac{H}{S} = \left\{ \frac{4\sinh kh}{kh} \frac{kh\sinh kh - \cosh kh + 1}{\sinh 2kh + 2kh} \right\}, \tag{12}$$

where H is the height of the progressive wave and S is the stroke of the wave-maker.

To verify the accuracy of waves produced in the 3D NWT, the results of the current method have been compared with the published experimental data of Zhao [10]. In that research, regular waves with an amplitude of 0.036 m and periods of 1 s have been generated using a plunger wave-maker.

In the first step, blockMesh function has been used to generate square blocks in the numerical domain. At this stage, the size of the cells is the same in both the X and Y directions, and only in the Z direction, a simple grading method has been applied to produce finer mesh around the free surface. To achieve a proper network in the regions around the hull (fixed cylinder or floating box), mesh refinement has been utilized. Several times within a cube, the cells become smaller and eventually The snappyHexMesh function is used to subtract the stl-format file from the solution domain.

In this paper, the method proposed by Celik et al. [29] has been used to analyze the uncertainty in the numerical solution. Representative grid size has been defined as:

$$h = \left[\frac{1}{N} \sum_{i=1}^{N} \left(\Delta V_i \right) \right]^{\frac{1}{3}}, \tag{13}$$

where ΔV_i is the volume of the ith cell and N is the total number of cells used for the computations. If $h_1 < h_2 < h_3$ and $r_{21} = h_2/h_1$ and $r_{32} = h_3/h_2$, then p can be defined by:

$$p = \frac{1}{\ln\left(r_{21}\right)} \left| \ln\left| \varepsilon_{32} / \varepsilon_{32} \right| + q(p) \right|,$$

$$q(p) = \ln\left(\frac{r_{21}^{p} - S}{r_{32}^{p} - S} \right),$$

$$S = 1 \cdot \operatorname{sgn}\left(\varepsilon_{32} / \varepsilon_{21} \right), \tag{14}$$

where $\varepsilon_{32} = R_3 - R_2$, $\varepsilon_{32} = R_3 - R_2$, and R_k denotes the solution on the kth grid. Here R means the average value of the wave height measured.

Equation (14) can be solved using an iterative method. Also, the extrapolated values are:

$$R_{ext}^{21} = \left(r_{21}^{p} R_1 - R_2 \right) / \left(r_{21}^{p} - 1 \right),$$

$$R_{ext}^{32} = \left(r_{32}^{p} R_2 - R_3 \right) / \left(r_{32}^{p} - 1 \right). \tag{15}$$

Finally, the error is estimated based on one of the following values:

Approximate relative error,

$$e_a^{21} = \left| \frac{R_1 - R_2}{R_1} \right|. \tag{16}$$

Extrapolated relative error,

$$e_{ext}^{21} = \left| \frac{R_{ext}^{12} - R_1}{R_{ext}^{12}} \right|. \tag{17}$$

Fine-grid convergence index,

$$GCI_{fin}^{21} = \frac{1.25 \cdot e_a^{21}}{r_{21}^{p} - 1}. \tag{18}$$

Finally, the uncertainty analysis obtained from Eq. (18) is presented in Table 4. The generated waves were evaluated in each gridding mode, and the mean value of the wave height was used to analyze the numerical solution uncertainty.

Therefore, it can be concluded that the uncertainty due to the numerical solution in the fine-grid solution for the mean wave height equal to 1.0%. Time histories of wave run-up at the longitudinal point of 3 m from wave-maker,

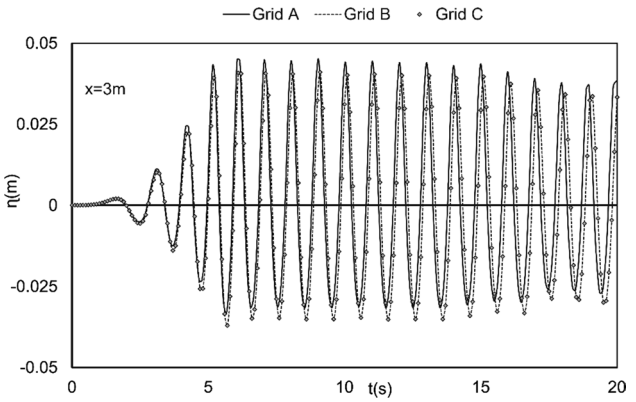

Fig. 2 Numerical result of regular wave amplitude generated in NWT based on different meshes

using three different mesh sizes, are shown in Fig. 2. According to the results presented in Table 4, which is based on the free surface elevation observed in Fig. 2, the B mode can be accepted as a suitable mesh for numerical analysis.

The results of free surface fluctuations at three different points of the numerical wave tank are compared with experimental data in Fig. 3. It can be observed that the result of generated waves at $x = 3$ m closely matched the surface elevation presented by Ming et al. [10]. When waves assess in further distance from the wave-maker, results begin to show the variation that is more significant from 7 m after the wave-maker. The highest dissimilarity of maximum amplitudes of generated waves between numerical and experimental methods, at $x = 3$ m from wave-maker for 20 s, is extremely about 5.8 percent. As a result, it has been concluded that the present wave-maker, at a proper distance, can generate suitable waves, which leads to obtaining accurate results in further analysis.

3.2 Regular wave interaction with a fixed truncated circular cylinder

For the second benchmark, a simple 3D case of regular waves, the height of 7.898 m and the period of 9s, passing over a submerged fixed vertical truncated circular cylinder, has been investigated. The geometric characteristics of this cylinder are presented in Table 3. In order to demonstrate that OpenFOAM is capable of simulating the propagation and transformation of surface water waves, a test case carried out with the scale of 1:50.3 by the Ocean Engineering Committee [21], has been performed here numerically using OpenFOAM and the results have been compared with each other (Fig. 4). NWT with the length of 16 m, width of 0.6 m, and height of 2 m with total cells of 2648723 is used to simulate this problem (Table 4).

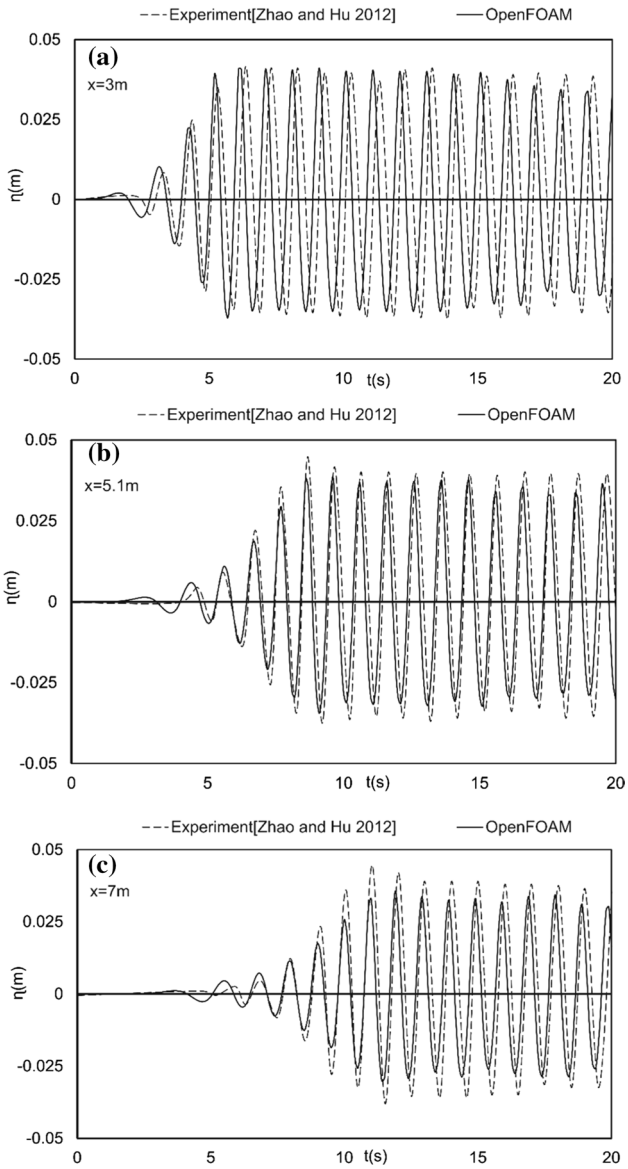

Fig. 3 Comparison of the numerical and experimental [10] wave elevation vs time at three different positions: **a** $x = 3$ m, **b** $x = 5.1$ m, **c** $x = 7$ m (amplitude = 0.036 m, period = 1 s)

The time history of the wave elevation is shown in Fig. 4. Additionally, the variation of the wave maximum amplitude between experimental and numerical data is presented in Table 5. For the time of 14.75 s, the maximum difference of the wave amplitude between the experimental and numerical solution results is about 5.19 percent. This difference in the negative quantity of wave amplitude reaches a maximum of 8.75 percent for 32.68 s after computation. For the positive wave amplitude, it has been determined that the simulated wave elevation is closer to the experimental solution, and the maximum variation occurred in the time of 29.47 s with a figure of 7.09 percent. The maximum difference, in the phase

Table 3 Main dimension of the fixed cylinder and the freely floating box

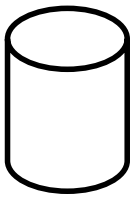

Parameter	Value (m)
Diameter	8
Draft	24
Height	45.27
Water Depth	75.45

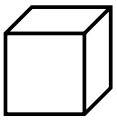

Parameter	Value (m)
Length	0.3
Draft	0.1
Height	0.2
Width	0.42
Water Depth(d)	0.4

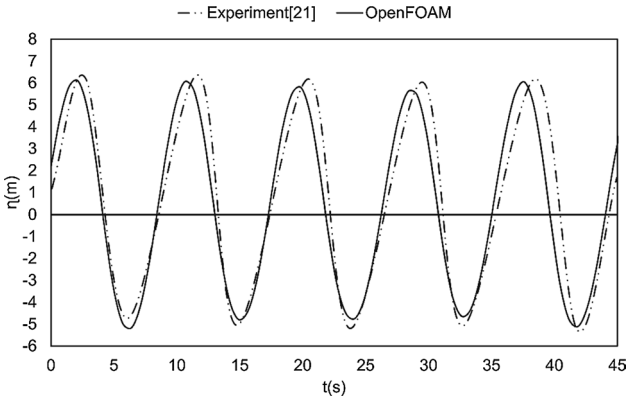

Fig. 4 Comparison of experimental [21] and numerical results for wave run-up around a fixed truncated circular cylinder at x=142.645 m of wave tank (H/L= 1/16, T= 9s)

between the experimental and numerical solution results, is approximately 3.7 percent. According to the results, the numerical prediction is in good agreement with the experimental measurement.

3.3 The regular wave interaction with a freely floating box

In the third case, a freely floating box with 6-DOF is exposed to waves with 0.12 m height and a period of 1 s in the water with a depth of 0.4 m. The dimension of NWT, in this case, is 16 m of length, 0.44 m of width, and 1 m of height. Total cells used in this numerical computation are counted 1,854,125. The comparison between the computational results and experimental data, for the heave motion of the freely floating box, is illustrated in

Table 4 Grid size for 3 different mesh procedures

No	Δx	Δy	Δz	Total cells	Run time	GCI_{fin}
A	0.035	0.035	0.035	672,120	10 h	0.24
B	0.03	0.03	0.03	983,600	16 h	0.05
C	0.02	0.03	0.02	1647,860	25 h	0.01

Table 5 The variation of wave run-up around a truncated circular cylinder in experimental and numerical methods

Experiment [21]		OpenFOAM		Time deviation (%)	Wave amplitude deviation (%)
Time(s)	Wave run-up (m)	Time(s)	Wave run-up (m)		
14.75	− 5.05	14.89	− 4.788	+ 0.95	− 5.19
20.45	6.179	19.85	5.788	− 2.9	− 6.32
23.77	− 5.196	24.11	− 4.75	+ 1.43	− 8.58
29.47	6.035	28.37	5.607	− 3.7	− 7.09
32.68	− 5.085	32.62	− 4.64	− 0.18	− 8.75
38.49	6.188	37.59	6.048	− 2.3	− 2.26
41.81	− 5.27	41.84	− 5.11	+ 0.07	− 3.03

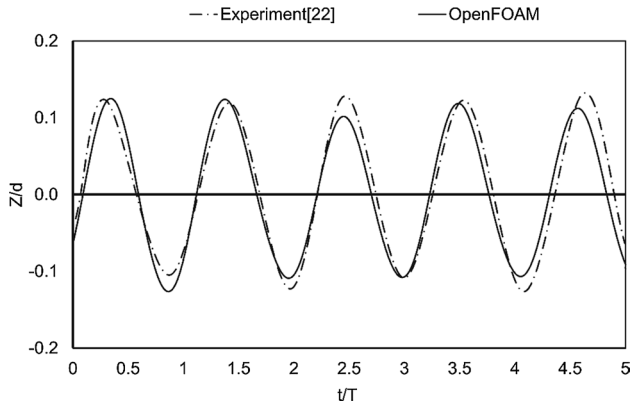

Fig. 5 Numerical and experimental [22] heave motions of the box exposed to the regular wave with height of 0.12 m and period of 1 s

Fig. 5. The number of cycles observed in this figure is selected based on experimental results. However, presenting more cycles does not show a difference in the numerical results.

The maximum quantity for dimensionless heave motion predicted in the OpenFOAM is + 0.11 and − 0.1, which is approximately equal to the results of the experimental method, with the value of + 0.12 and − 0.1. It can be seen that the numerical model accurately predicted the normalized heave motion for the studied case in comparison with the experimental solution.

4 Result and discussion

After ensuring the accuracy of the wave generated in the tank and also examining the ability of this numerical method to simulate the free surface and dynamics of a floating body in water, the dynamic behavior of a floating cylinder will be evaluated under different conditions.

4.1 A 6-DOF freely floating truncated circular cylinder in regular waves

Computational prediction of the interaction between small-amplitude regular waves and the floating circular cylinder, operating in deep water with no movement restriction, is carried out in this section. The main interests are the results of motions of the floating cylinder and forces acting on it. Small-amplitude regular waves, with a full-scale wave height of 4.777 m and a wave period of 7 s, are generated in the water with a depth of 51.66 m. Numerical simulations are carried out in OpenFOAM, utilizing a 3-D NWT (length of 16 m, a width of 0.6 m, and height of 2 m) and a scaled floating cylinder (1:50.3), located at $x = 3$ m from the wave-maker. The initial time step is 0.01 s and dynamically determined to satisfy the criterion of the maximum courant number of 0.5 and the total simulation time up to 15 s.

A grid convergence study for heave motion of the cylinder is carried out with five different grid sizes: $\Delta x = \Delta z = 0.1$, $\Delta x = \Delta z = 0.035$, $\Delta x = \Delta z = 0.025$, $\Delta x = \Delta z = 0.02$, and $\Delta x = \Delta z = 0.015$. For all cases, $\Delta y = 0.05$. A hexahedral mesh is used to simulate NWT and the cylinder. Besides, fine grids are used in regions close to the free surface and around the cylinder to increase the precision of results (0.2 m below and above the free surface; 0.3 before and after and below and above the cylinder). The schematic of the mesh arrangement, considering the cylinder and the damper, is presented in Fig. 6. After considering the mesh refinement, the intermediate mesh ($\Delta x = \Delta z = 0.02$ and $\Delta y = 0.05$) with the longitudinal cell number of 800, vertical number of 90, and transverse cell number of 12 (total 2,862,040 cells) is selected in accordance with the accuracy of the result, the number of cores in which the case has been running (Corei7-6700@4GHZ with 12 GB of memory) and the corresponding total run time (42 h). The main variables of interest in this study are surge and heave motions of the cylinder and drag and lift wave forces and also the pitch

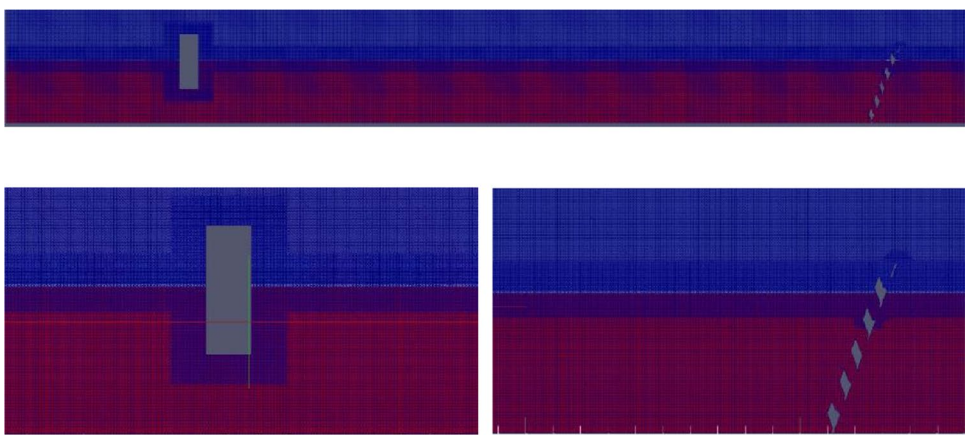

Fig. 6 Schematic of grid arrangement in OpenFOAM (color)

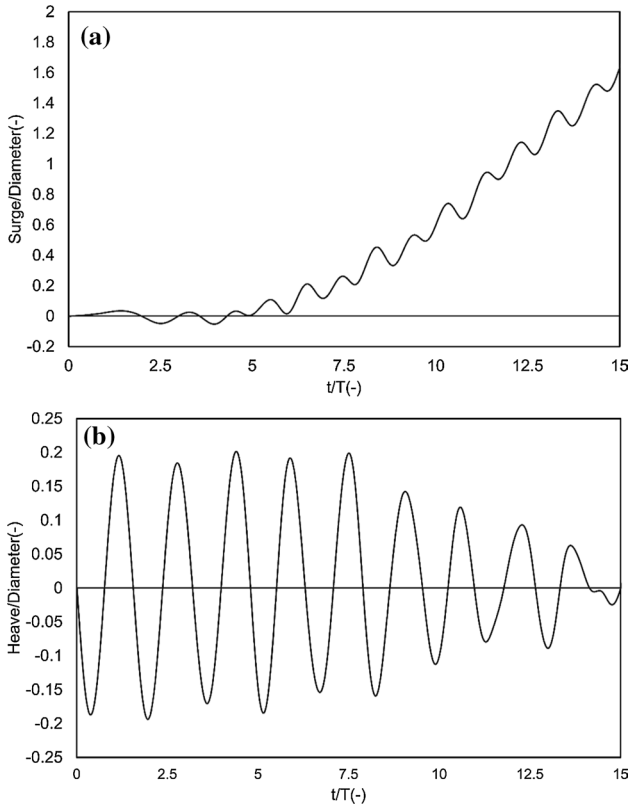

Fig. 7 Normalized surge and heave motion of the freely floating cylinder exposed to the wave with height of 4.777 m and period of 7 s

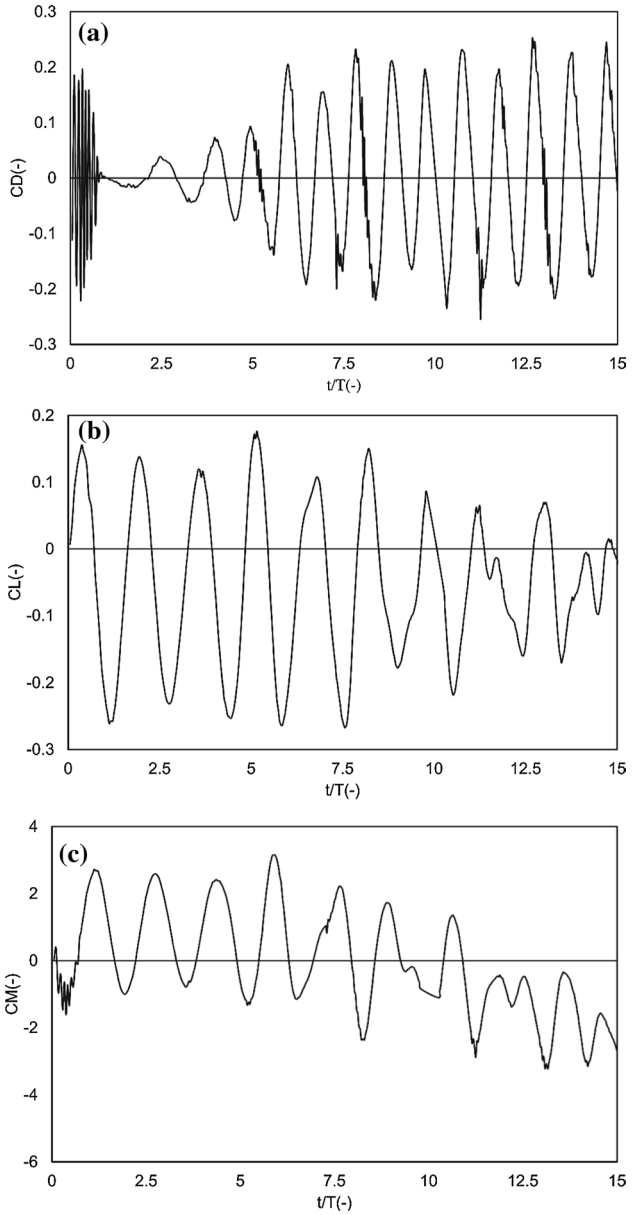

Fig. 8 Wave normalized induced forces acting on a freely floating cylinder exposed to wave with height of 4.777 m and period of 7 s: **a** Drag, **b** Lift, **c** Pitch

moment acting on it. Normalized motion results of the floating circular cylinder with full-scale dimension in the regular wave with a height of 4.777 m and period of 7 s moving in the water with a depth of 51.66 m are illustrated in Fig. 7.

Figure 7 shows the dimensionless surge and heave responses of the floating cylinder exposed to regular waves. It is obvious from Fig. 7a that the cylinder leaves its initial longitudinal location at a slow speed and fluctuating rate. The gradient of variation is about 2.6 percent up to 7.5 of the normalized time. After that, the cylinder has a significant shift to forward from 7.5 to 15. These differences are entirely noticeable, relocating the cylinder horizontally from its initial place to about 7.36 percent. This approach has an impact on the vertical oscillation of the cylinder too (Fig. 7b). The cylinder begins to fluctuate periodically with almost the constant amplitude during the first 7.5 of the unitless time. The maximum amplitude of normalized vertical movement within this period reaches about 0.2.

Figure 8a, b shows the drag and lift force coefficients induced on the freely floating cylinder by regular waves. It is obvious from Fig. 8a that the drag force coefficient tends to fluctuate with a constant positive and negative value between about − 0.2 to + 0.2. In contrast, the lift force acting on the cylinder tends to move toward negative quantities, such that it peaks at approximately + 0.15 and − 0.25 in positive and negative directions, respectively.

Figure 8c shows that the value of pitch moment on the cylinder exposed to regular waves in deep water is significant. The maximum dimensionless magnitude of that gets to around + 2.5. The maximum amplitude of the negative pitch moment influences the cylinder after the unitless time of 10. The cylinder encountered with positive pitch moment rather than the negative one up to 7.5. But over

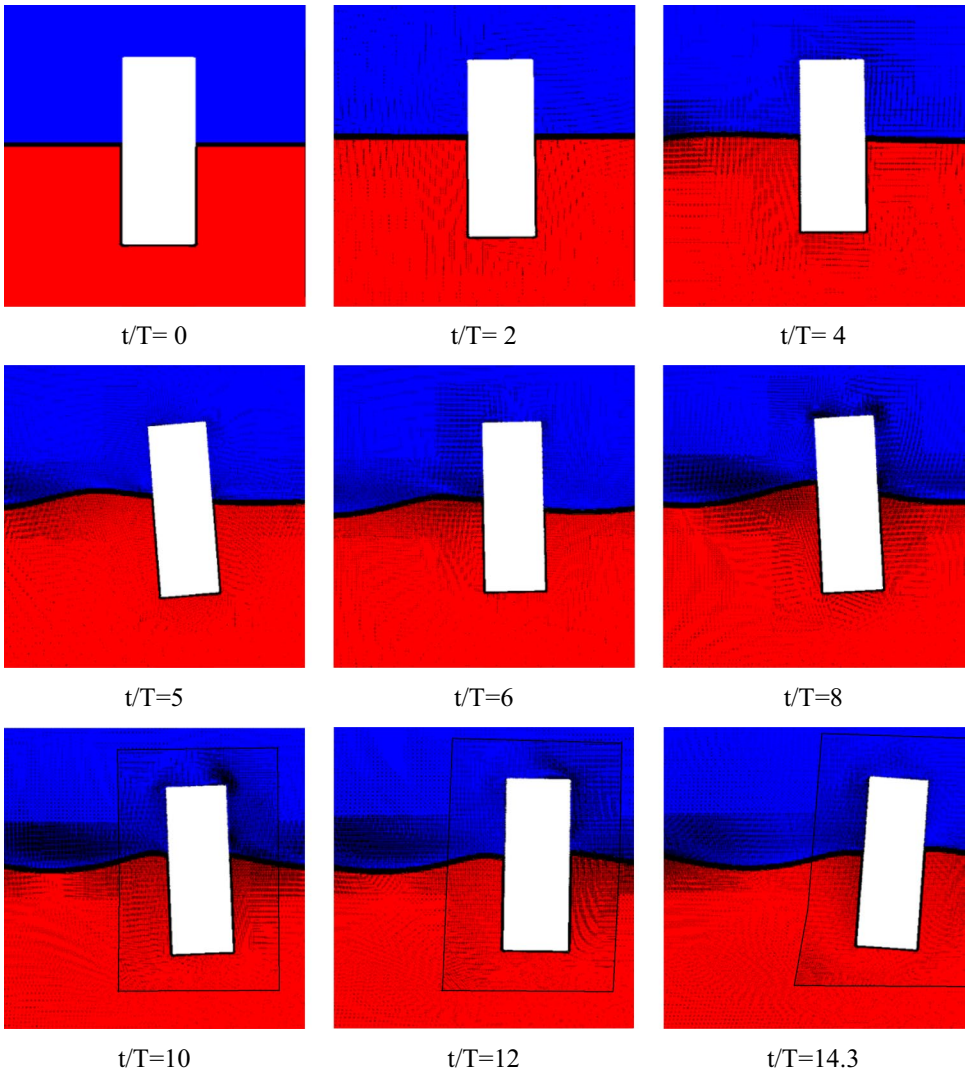

Fig. 9 Schematic of the interaction between regular waves and the truncated circular cylinder during time (color)

time, the condition changes, and just the negative pitch moment affects the movement of the cylinder.

The graphical view of the interaction of small-amplitude regular waves and the circular cylinder over time is shown in Fig. 9. In each time step, the situation of the body in regular waves and the extension of the snappy mesh due to the propagation of the wave and the cylinder are presented. In the bottom row images, black lines are used to show the moving mesh area more clearly.

4.2 The effect of the water depth on the freely floating truncated circular cylinder

The final part of the analysis includes the response of the floating cylinder to the change in the water depth from deep to intermediate. This is expected that the distance of the circular cylinder from the seafloor affects motions of the cylinder and also forces acting on it. To explore this issue, five different depths of 31.54, 34.05, 51.66, 64.24, and 76.81 m are chosen, and results of the dimensionless surge and heave motions of the cylinder and additionally the induced hydrodynamic force coefficients are provided in Figs. 10 and 11, respectively.

Figure 10a, b illustrates the cylinder's center of gravity movement in horizontal and vertical directions when the depth of water varies. It is obvious from Fig. 10a that the normalized surge motion of the cylinder tends to have a similar trend in figures in the first 7 dimensionless periods of the test, while depths change. The freely floating cylinder moves 1.5 percent from its initial location during this period. As time passes, graphs become divergent, and the slope of differences increases, while the water becomes deeper. As an instance, the longitudinal location of the cylinder heightens to over 9.6 percent for the depth of 76.81 m compared with around 4.4 percent for 31.54 m of the water depth after the unitless time of 15. On the other hand, vertical oscillations of the cylinder in regular waves fall when vertical distances from the bottom

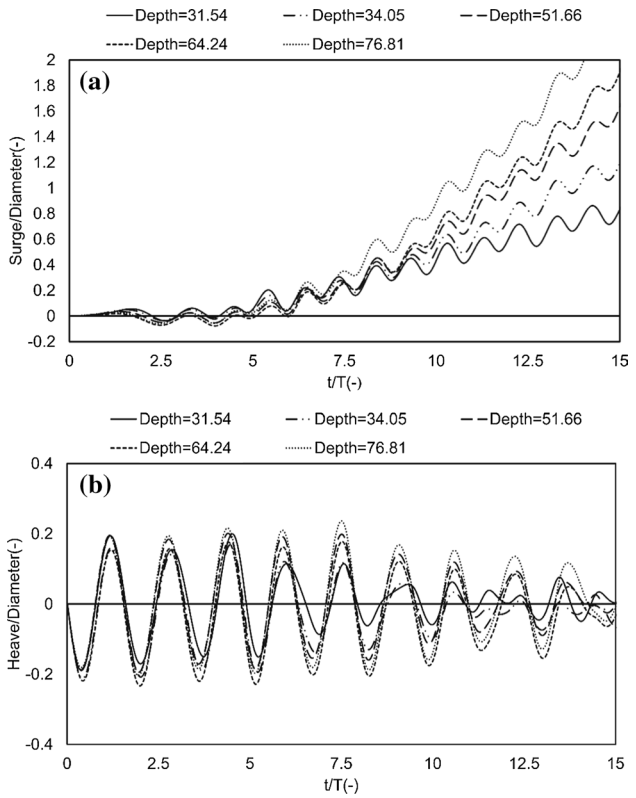

Fig. 10 Normalized surge and heave motions of the freely floating cylinder in different water depths ($H = 4.777$ m, $\underline{T} = 7$ s)

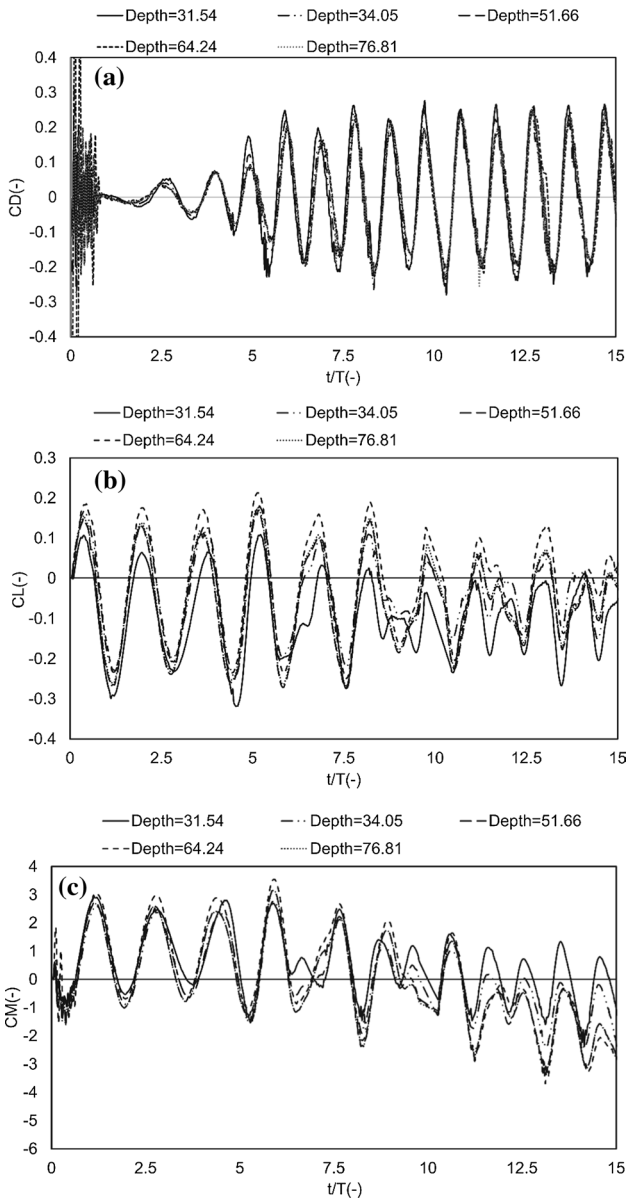

Fig. 11 Normalized drag and lift forces and pitch moment of the freely floating cylinder in different depths

decrease. Figure 10b displays that the amplitude of heave motion for the cylinder moving in deep water increases noticeably. In dimensionless time 5.9, the maximum normalized amplitude of the heave motion peaks at 0.21 for the depth of 76.81 m, while this figure falls to 0.11 for the finite depth of 31.54 m. In fact, in a condition that the bottom of the cylinder is in the vicinity of the seafloor (depth of 31.54 m), regular waves push the cylinder up and down between − 0.15 and 0.2, while these numbers tend to increase in deep water from − 0.2 to 0.2 in the water depth of 76.81 m with having dissimilar amplitude when time goes by. These susceptibilities can be observed in forces too.

Figure 11a indicates that drag force coefficients have similar trends in all water depths and differences are negligible. The amplitude of this coefficient varies between − 0.2 and + 0.22 for different depths. In contrast, lift force coefficients show noticeable increases in lower depths, rises sharply to a peak of + 167 in the depth of 31.54 compared to + 0.07 for the depth of 76.81 m. This trend followed by the other depths the cylinder probed in. According to Fig. 11c, changes in pitch moment values are considerable when the water depth varies. However, the rate of this variation is less than that for the lift force the positive pitch moment rises in content in comparison with its negative amplitude in shallower waters. As a whole, it is expected that the floating circular cylinder is to have dissimilar trends in vertical motions and forces when it is near the seafloor.

5 Conclusion

The current study was focused on the stimulation of a NWT with a moving wall wave-maker, in OpenFOAM. Using a moving mesh technique based on a fixed number of cells has led to an increase in problem-solving accuracy along with a reduction in computational time. Some benchmarks were employed to verify the current numerical method.

Throughout the comparison, the proper agreement was demonstrated between the proposed numerical model and the experimental measurement. Eventually, the response of a freely floating cylinder in regular waves and different water depths was investigated. From the simulations, the following conclusions can be drawn:

- The proposed NWT, paddle wave-maker, and modified grid approach utilizing moving mesh (SnappyHexMesh) provide acceptable results in the case of capturing the free surface effect and dynamic behavior.
- The main scope of the current study is to introduce a physical wave-maker, generating desired regular waves. For this purpose, some comparisons were carried out, between the results obtained using a moving wall wave-maker, and the results of published experimental data.
- The study on the interaction of the regular wave with a floating cylinder with 6-DOF demonstrated that the performance of the cylinder in deep water is desirable. Although the movement of dynamic grids with objects plays an important role in the accuracy of results, selecting a proper distance of a floating object from the wave-maker has to be considered as another factor in analyzing.
- Finally, the response of the freely floating cylinder was explored in different water depths. It was found that the water depth has a significant effect on the heave motion. At the higher depth of the water, the vertical movement was more satisfactory and had a similar trend in the maximum value during the time (average maximum amplitude of 0.35 for the depth of 76.81 m). This scheme was confirmed for the lift force and pitch moment too. On the other hand, when the floating object goes to a region with less depth, the seafloor causes disturbances of generated waves and also prevents the proper functioning of the floating body by affecting it. For instance, the floating cylinder presented dissimilarity in quantity in the depth of 31.54 m (the maximum amplitude of the normalized heave motion changed from 0.3 to about 0.06 during the time).

Although the scale and geometry considered in the current research may not be directly practical to determine the hydrodynamic behavior of an offshore structure, the verification of such a model provides the first step toward establishing such methods to an eventual application to larger and more complex problems, with realistic geometries, enduring critical situations.

Endnote

C_D	Drag force coefficient (–)	$\frac{F_D}{0.5\cdot\rho\cdot A_{ref}\cdot U^2}$
C_L	Lift force coefficient (–)	$\frac{F_L}{0.5\cdot\rho\cdot A_{ref}\cdot U^2}$
C_M	Pitch moment coefficient (–)	$\frac{F_M}{0.5\cdot\rho\cdot A_{ref}\cdot L_{ref}\cdot U^2}$
A_{ref}	Cylinder cross-sectional area (m^2)	$\frac{\pi}{4}D^2$
L_{ref}	Cylinder diameter (m)	D
U	Wave velocity (m/s)	
L	Wave length (m)	–
T	Wave period (s)	–

References

1. Ghadimi P, Paselar Bandari H, Bakhshandeh Rostami A (2012) Determination of the heave and pitch motions of a floating cylinder by analytical solution of its diffraction problem and examination of the effects of geometric parameters on its dynamics in regular waves. Int J Appl Math Res 1(4):611–633. https://doi.org/10.14419/ijamr.v1i4.396
2. Finnegan W, Meere M, Goggins J (2011) The wave excitation forces on a floating vertical cylinder in water of infinite depth. In: World renewable energy congress, May 8–13, Linkoping, Sweden, pp 2175–2182. https://doi.org/10.3384/ecp110572175
3. Finnegan W, Meere M, Goggins J (2013) The wave excitation forces on a truncated vertical cylinder in water of infinite depth. J Fluids Structs 40:201–213. https://doi.org/10.1016/j.jfluidstructs.2013.04.007
4. Yao WJ, Liu Y, Qiu YZ (2015) An analytical solution for the diffraction problem of a submerged vertical cylinder considering bottom-mounted barrier effect. J the Chin Inst Eng 38(6):1–11. https://doi.org/10.1080/02533839.2015.1016876
5. Koo W, Kim MH (2004) Freely floating-body simulation by a 2D fully nonlinear numerical wave tank. Ocean Eng 31(16):2011–2046. https://doi.org/10.1016/j.oceaneng.2004.05.003
6. Bai W, Taylor RE (2007) Numerical simulation of fully nonlinear regular and focused wave diffraction around a vertical cylinder using domain decomposition. Appl Ocean Res 29(1–2):55–71. https://doi.org/10.1016/j.apor.2007.05.005
7. Bai W, Taylor RE (2009) Fully nonlinear simulation of wave interaction with fixed and floating flared structures. Ocean Eng 36(3–4):223–236. https://doi.org/10.1016/j.oceaneng.2008.11.003
8. Abbasnia A, Ghiasi M (2014) A fully nonlinear wave interaction with an array of submerged cylinders by NURBS numerical wave tank and acceleration potential. Ships Offshore Struct 9(4):404–417. https://doi.org/10.1080/17445302.2013.819688
9. Song X, Shibata K, Nihei Y, Koshizuka S (2015) Numerical analysis of the wave force acting on a cylinder in regular waves using the MPS method. Comp Part Mech 3(1):83–93. https://doi.org/10.1007/s40571-015-0096-x
10. Zhao X, Hu C (2012) Numerical and experimental study on a 2-D floating body under extreme wave Conditions. Appl Ocean Res 35:1–13. https://doi.org/10.1016/j.apor.2012.01.001
11. Repalle N, Thiagarajan K, Paterson F (2010) Wave run up investigation on a square cylinder. 17th Australasian Fluid Mechanics Conference, December. Auckland, New Zealand, pp 5–9
12. Nematbakhsh A, Gao Z, Moan T (2016) Benchmarking of a CFD based numerical wave tank for studying wave load effects on fixed and floating offshore structures. J Offshore Mech Arct Eng 139(3):1–16. https://doi.org/10.1115/1.4035475
13. Lin YH, Chen JF, Lu PY (2017) A CFD model for simulating wave run-ups and wave loads in case of different wind turbine foundations influenced by nonlinear waves. Ocean Eng 129:428–440. https://doi.org/10.1016/j.oceaneng.2016.10.050

14. Bharath A, Nader JR, Pensis I, Macfarlane G (2018) Nonlinear hydrodynamic effects on a generic spherical wave energy converter. Renew Energy 118:56–70. https://doi.org/10.1016/j.renene.2017.10.078
15. Chen LF, Zang NJ, Hillis AJ, Morgan GCJ, Plummer AR (2014) Numerical investigation of wave–structure interaction using OpenFOAM. Ocean Eng 88:91–109. https://doi.org/10.1016/j.oceaneng.2014.06.003
16. Chen L, Zhou J (2015) Analyses of wave forces on surface piercing vertical cylinders of intermediate scale. Procedia Eng 126:290–294. https://doi.org/10.1016/j.proeng.2015.11.245
17. Hu ZZ, Greaves D, Raby A (2016) Numerical wave tank study of extreme waves and wave-structure interaction using OpenFOAM. Ocean Eng 126:329–342. https://doi.org/10.1016/j.oceaneng.2016.09.017
18. Ye H, Wan D (2017) Benchmark computations for flows around a stationary cylinder with high Reynolds numbers by RANS-overset grid approach. Appl Ocean Res 65:315–326. https://doi.org/10.1016/j.apor.2016.10.010
19. Wang J, Wan D (2018) CFD investigation of ship maneuvering in waves using naoe-FOAM-JSTU solver. J Mar Sci Appl 17(3):443–458. https://doi.org/10.1007/s11804-018-0042-4
20. Huang Y, Cheng P, Decheng Wan (2019) Numerical analysis of a floating offshore wind turbine by coupled Aero-Hyrodynamic simulation. J Marine Sci Appl 18(1):82–92. https://doi.org/10.1007/s11804-019-00084-8
21. Ocean Engineering Committee (2014) Final report and recommendations to the 27th ITTC. Denmark: Copenhagen
22. Ming H, Bing R, Da-hong Q (2016) Experimental study of nonlinear behaviors of a free-floating body in waves. China Ocean Eng 30(3):421–430. https://doi.org/10.1007/s13344-016-0018-6
23. Dao MH, Chew LW, Zhang Y (2018) Modelling physical wave tank with flap paddle and porous beach in OpenFOAM. Ocean Eng 154:204–215. https://doi.org/10.1016/j.oceaneng.2018.02.024
24. Dai S, Younis BA, Sun L (2015) OpenFOAM predictions of hydrodynamics loads on full-scale TLP. Ocean Eng 102:162–173. https://doi.org/10.1016/j.oceaneng.2015.04.042
25. Higuera P, Losada IJ, Lara JL (2015) Three-dimensional numerical wave generation with moving boundaries. Coast Eng 101:35–47. https://doi.org/10.1016/j.coastaleng.2015.04.003
26. Chenari B, Saadatian SD, Ferreira A (2015) Numerical Modelling of Regular Waves Propagation and Breaking Using Waves2Foam. Clean Energy Technol 3(4):276–281. https://doi.org/10.7763/jocet.2015.v3.208
27. Berberović E, VanHinsberg NP, Jakirlić S, Roisman IV, Tropea C (2009) Drop impact on to a liquid layer of finite thickness: dynamics of the cavity evolution. Phys Rev E 79(3):1–13. https://doi.org/10.1103/physreve.79.036306
28. Panahi R, Jahanbakhsh E, Seif MS (2009) Towards simulation of 3D nonlinear high-speed vessels motion. Ocean Eng 36:256–265
29. Celik I, Ghia U, Roache PJ, Freitas CJ, Coleman H, Raad PE (2008) Procedure of estimation and reporting of uncertainty due to discretization in CFD applications. J Fluids Eng-Trans ASME 130(7):078001-1